A Treatment for Overlapping Fractures in the Context Of Mixed Finite Elements for Flow in Fractured Porous Media

Nathan Shauer[1], José B. Villegas S.[2], Philippe R. B. Devloo[1]

[1]*School of Civil Engineering, Unicamp*
R. Josiah Willard Gibbs 85 - Cidade Universitaria, Campinas SP, Brazil, CEP 13083-839
shauer@unicamp.br, phil@unicamp.br
[2]*Faculdade de Ciencias de la Ingeniería*
Universidad Estatal Peninsula de Santa Elena, Santa Elena, 240204, Ecuador
jvillegas@upse.edu.ec

Abstract. Accurately modeling flow in discrete fracture networks (DFNs) can be important for several fields of engineering such as groundwater management, petroleum engineering, and geotechnical engineering where these DFNs can play a key role in the flow patterns in a formation. These fracture networks are often complex and can have fractures in very close proximity, which, in turn, can lead to challenges in creating fitting meshes for finite element analyses. This work proposes a methodology to handle overlapping fractures in the context of simulating flow in fractured porous media using a Mixed Finite Element Method formulation. With this capability, fractures in close proximity can simply occupy the same geometric location in the mesh, which avoids the creation of elements with poor aspect ratio. In this work, the porous media flow is modeled with traditional Darcy's equations and the fractures and their interaction with the porous media are modeled using the Discrete-Fracture-Matrix (DFM) representation. A mixed finite element formulation is adopted to solve the flow problem in both porous media and fractures, which has key features such as local mass conservation and improved velocity approximation. The mesh generation is done using the DFNMesh algorithm, which is a mesh generator for DFNs that can handle overlapping fractures by using pre-defined user settings. The proposed methodology is analyzed using a set of numerical examples, which show the importance of the treatment even for very simple cases and that it can handle overlapping fractures and provide accurate results for the flow in complex fractured porous media problems.

Keywords: Discrete fracture-matrix model, Discrete Fracture Networks, Mixed finite elements, Porous media flow

1 Introduction

More than half of the Earth's continental surface is covered by low-permeability rocks, which impede fluid flow in the reservoir matrix [1]. Fracturing these rocks can significantly enhance their permeability, and given that approximately 65% of oil reserves [2] are also located in naturally fractured reservoirs, it is essential to develop a reservoir simulator that considers the secondary permeability introduced by fractures. This additional permeability greatly influences the flow patterns within the porous media.

The Discrete-Fracture-Matrix (DFM) model has emerged as an increasingly popular technique for simulating flow in fractured porous media [3, 4]. In the DFM framework, fractures are depicted as lower-dimensional elements at the interfaces of matrix finite elements. Although this model accurately captures the physical behavior, it poses challenges for meshing algorithms in finite element approximations. Fractures act as constraints, leading to overly fine meshes or elements with poor aspect ratios. Therefore, achieving a robust and adaptable discretization for DFM modeling remains a significant challenge [5].

Various discretization methods have been proposed to solve the equations associated with DFM modeling of fracture networks. These methods include the Finite Element Method (FEM) [6], Discontinuous Galerkin Methods (DG) [7], Finite Differences Methods (FD) [8], Finite Volume Methods (FVM) [9], Virtual Element Methods [10], Generalized/eXtended Finite Element Methods (G/XFEM) [11], Mixed Finite Element techniques [5, 12], the Cut Finite Element Method (CutFEM) [13], and the Embedded Finite Element Method (EFEM) [14]. Each of these techniques offers unique benefits and challenges. Benchmark problems have been developed and analyzed to compare the effectiveness of these methods, demonstrating ongoing advancements in this area [15, 16].

This work examines fluid flow in discrete fracture networks using a locally conservative and stable mixed finite element method [12, 16, 17]. Some advantages of the method are its local mass conservation and strong enforcement of divergence-free conditions for incompressible flows. This method is therefore crucial for coupling fluid flow with transport problems such as heat and saturation in multiphase flows. The methodology involves generating conforming meshes in complex fracture networks without excessive refinement. For that, the DFNMesh algorithm [18] is employed and a methodology to handle overlapping fractures while maintaing accuracy and stability is developed and explored. Through a benchmark problem, the performance of this approach is evaluated, showcasing its capability in accurately simulating flow in fractured porous media even with coarse meshes.

2 Methodology

2.1 Constitutive treatment for merged fractures during discretization

When fractures are very close together, the snapping tolerances of the DFNMesh algorithm may cause them to be merged into a single location within the generated Finite Element mesh. This merging neglects the influence of the porous matrix between these fractures. Figure 1 illustrates this issue with an initial coarse mesh composed of two hexahedral elements. In this example, the DFNMesh algorithm uses two fractures (depicted in blue and red) to create a conforming mesh. The fractures are located at distances l_{d1} and l_{d2} from the interface between elements of the initial coarse mesh. Based on the chosen tolerance in DFNMesh, these fractures can either refine the initial mesh into four hexahedral elements or merge into a single location within the initial mesh. If merging occurs, the porous media's effect between the fractures would be disregarded.

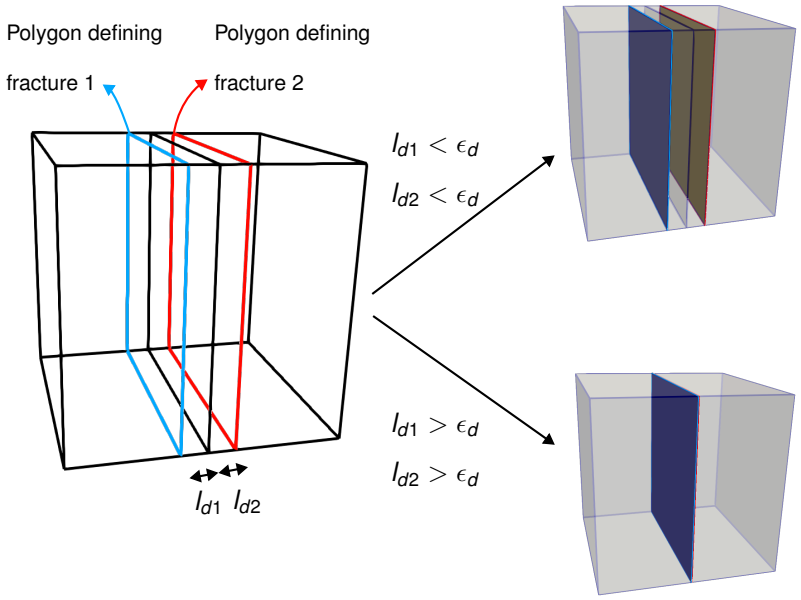

Figure 1. The DFNMesh algorithm can encounter issues with overlapping fractures when generating Finite Element meshes. Depending on the adopted snapping tolerances, fractures labeled as 1 and 2 may end up overlapping at the same location within the generated mesh.

To preserve critical flow characteristics, the perpendicular flux $u_{(ij)}$ between two overlapping fractures i and j is explicitly modeled. The fluid exchange between these fractures is governed by the following constitutive law:

$$u_{(ij)} = -K_{(ij)} \frac{(p_{2,i} - p_{2,j})}{d_{(ij)}} \tag{1}$$

where $K_{(ij)}$ is the hydraulic conductivity of the porous media normal to both fractures, while $p_{2,i}$ and $p_{2,j}$ are the pressures at the respective points on fractures i and j. The term $d_{(ij)} = d_{(ij)}(\mathbf{x})$ represents the actual distance between the fractures. Figure 2 visually explains these variables. It is important to highlight that this approach only considers the flow that is perpendicular to the fractures.

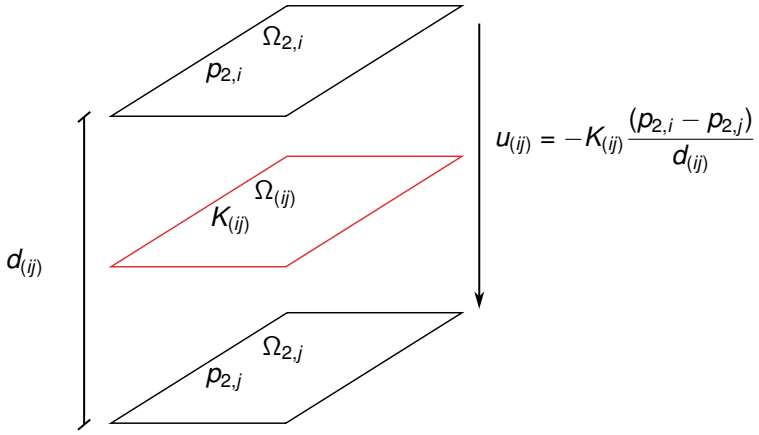

Figure 2. Constitutive treatment for overlapping fractures involves addressing fractures i and j, which have domains $\Omega_{2,i}$ and $\Omega_{2,j}$, respectively. Although these fractures overlap in the generated Finite Element mesh, they originally maintain a distance $d_{(ij)}$ between them. To account for the porous media's effect between these fractures, a flux variable $u_{(ij)}$ is introduced.

2.2 Governing equations

In [12], the mixed weak formulation of the governing equations is outlined for two-dimensional DFM scenarios. This paper extends that formulation to three-dimensional problems. The key distinction in 3D is that intersections between 2D fractures occur in one-dimensional spaces.

The $\mathrm{H}(\mathrm{div}, \Omega_d)$ and $L^2(\Omega_d)$ spaces have their usual meaning:

$$\mathrm{H}(\mathrm{div}, \Omega_d) = \left\{ \varrho_i \in L^2(\Omega_d); \mathrm{div}(\boldsymbol{\varrho}) \in L^2(\Omega_d) \right\} \quad d = 2, 3 \tag{2}$$

$$L^2(\Omega_d) = \left\{ f : \int_{\Omega_d} f^2 \, d\Omega_d < \infty \right\} \quad d = 1, 2, 3 \tag{3}$$

The following sets are defined for the weak form:

$$\mathcal{V}(\Omega_d) = \left\{ \boldsymbol{v} \in \mathrm{H}(\mathrm{div}, \Omega_d); \boldsymbol{v} \cdot \mathbf{n} \mid_{\partial\Omega_{d_N}} = 0 \right\} \quad d = 2, 3 \tag{4}$$

$$\mathcal{U}(\Omega_d) = \left\{ \mathbf{u} \in \mathrm{H}(\mathrm{div}, \Omega_d); \mathbf{u} \cdot \mathbf{n} \mid_{\partial\Omega_{d_N}} = u_{d_N} \right\} \quad d = 2, 3 \tag{5}$$

The full weak form of the problem is detailed in equations (6) to (11). The new terms associated with the overlap are highlighted in red. The weak form of the governing equations is: Find $(p_3, \mathbf{u}_3, p_2, \mathbf{u}_2, p_1) \in L^2(\Omega_3) \times \mathcal{U}(\Omega_3) \times L^2(\Omega_2) \times \mathcal{U}(\Omega_2) \times \mathrm{H}^{1/2}(\Omega_1)$ such that:

$$\int_{\Omega_3} \widetilde{\mathbf{u}}_3 \cdot \left(\mathbf{K}_3^{-1} \right) \mathbf{u}_3 \, d\Omega_3 - \int_{\Omega_3} \nabla \cdot \widetilde{\mathbf{u}}_3 \, p_3 \, d\Omega_3 + \int_{\partial\Omega_3^f} \left(\widetilde{\mathbf{u}}_3 \cdot \mathbf{n}_f \right) p_2 \, d\partial\Omega_3^f + \int_{\Omega_2} K_{tr} \left(\widetilde{\mathbf{u}}_3 \cdot \mathbf{n}_{\Gamma_2} \right) \left(\mathbf{u}_3 \cdot \mathbf{n}_{\Gamma_2} \right) \, d\Omega_2 + \int_{\partial\Omega_{3_D}} \left(\widetilde{\mathbf{u}}_3 \cdot \mathbf{n}_3 \right) \, p_{3_D} \, d\partial\Omega_{3_D} = 0 \qquad \forall \widetilde{\mathbf{u}}_3 \in \mathcal{V}(\Omega_3) \tag{6}$$

$$- \int_{\Omega_3} \widetilde{p}_3 \nabla \cdot \mathbf{u}_3 \, d\Omega_3 = 0 \qquad \forall \widetilde{p}_3 \in L^2(\Omega_3) \tag{7}$$

$$\int_{\Omega_2} \widetilde{\mathbf{u}}_2 \cdot \left(\frac{1}{a_2} \mathbf{K}_2^{-1} \right) \mathbf{u}_2 \, d\Omega_2 - \int_{\Omega_2} \nabla \cdot \widetilde{\mathbf{u}}_2 \, p_2 \, d\Omega_2 + \int_{\Omega_1} p_1 \left(\widetilde{\mathbf{u}}_2 \cdot \mathbf{n}_{1j} \right) \, d\Omega_1 + \int_{\partial\Omega_{2_D}} \left(\widetilde{\mathbf{u}}_2 \cdot \mathbf{n}_2 \right) \, p_{2_D} \, d\partial\Omega_{2_D} = 0 \qquad \forall \widetilde{\mathbf{u}}_2 \in \mathcal{V}(\Omega_2) \tag{8}$$

$$- \int_{\Omega_2} \widetilde{p}_2 \nabla \cdot \mathbf{u}_2 \, d\Omega_2 + \int_{\partial\Omega_3^f} \widetilde{p}_2 \left(\mathbf{u}_3 \cdot \mathbf{n}_f \right) \, d\partial\Omega_3^f + \int_{\Omega_{(ij)}} \widetilde{p}_2 u_{(ij)} s_{(ij)} \, d\Omega_{(ij)} = 0 \qquad \forall \widetilde{p}_2 \in L^2(\Omega_2) \tag{9}$$

$$\int_{\Omega_1} \widetilde{p}_1 \sum_j \mathbf{u}_2 \cdot \mathbf{n}_{1j} \, d\Omega_1 = 0 \qquad \forall \widetilde{p}_1 \in L^2(\Omega_1) \tag{10}$$

$$\int_{\Omega_{(ij)}} K_{(ij)}^{-1} d_{(ij)} u_{(ij)} \widetilde{u}_{(ij)} \, d\Omega_{(ij)} + \int_{\Omega_{(ij)}} (p_{2,i} - p_{2,j}) \widetilde{u}_{(ij)} \, d\Omega_{(ij)} = 0 \qquad \forall \widetilde{u}_{(ij)} \in L^2(\Omega_{ij}) \tag{11}$$

where $K_{tr} = \frac{a_2}{2K_2^{eq}}$, $\widetilde{\mathbf{u}}_3$ is the test function for matrix velocity, and $\widetilde{p}_3$ is the test function for matrix hydraulic head. Similarly, $\widetilde{\mathbf{u}}_2$ and $\widetilde{p}_2$ are the test functions for fracture fluid flow and fracture fluid hydraulic head, respectively. The domain of fracture intersections is represented by Ω_1, with p_1 denoting the fluid hydraulic head at a fracture intersection and $\widetilde{p}_1$ as the corresponding test function. The vector $\mathbf{n}_{1j}$ is tangent to fracture j at the intersection. Equation (10) asserts that the sum of fracture fluxes at an intersection must be zero, indicated by the summation symbol $\sum$, which accounts for the possibility of more than two fractures intersecting at the same location. The third term in Equation (6) is evaluated over the boundary $\partial\Omega_3^f$, covering both faces of the fracture. The sign function $s_{(ij)}$ equals 1 if fracture i is the first fracture in the overlap region and -1 if it is not. In cases of overlap, the region $d\partial\Omega_3^f$, which typically represents the two faces of a given fracture, only includes the faces that are not within the overlapping area. The chosen approximation spaces – H(div) for velocity/flow and L^2 for hydraulic head – are noted for their stability and essential properties, such as local mass conservation and strong divergence enforcement [17].

3 Examples

3.1 Two overlapping fractures

This example features two fractures that may partially overlap within the generated Finite Element mesh, contingent upon the snapping tolerances set for the DFNMesh algorithm. Illustrated in Figure 3a are the problem domain and boundary conditions. The material properties adopted are $\mathbf{K}3 = \mathbf{I}$, m/s (where $\mathbf{I}$ is the identity matrix), $\mathbf{K}2 = 10^3, \mathbf{I}, \mathrm{m}^3/s, K_2^{eq} = 10^4$, m/s, and $a_2 = 10^{-1}$, m. The initial coarse mesh used for the DFNMesh algorithm is depicted in Figure 3b, while the snapped and non-snapped generated meshes are shown in Figure 4. The analysis includes three scenarios regarding the overlap of fractures in the generated Finite Element mesh. In the first scenario, the permeability of the porous media between the fractures ($K_{(ij)}$) is assigned the actual value of the porous media. In the second scenario, $K_{(ij)}$ is set to a very high value, simulating two fractures sharing the same pressure in the overlapping region. In the third scenario, $K_{(ij)}$ is given a very low value, representing fractures that do not exchange flow in the overlapping region.

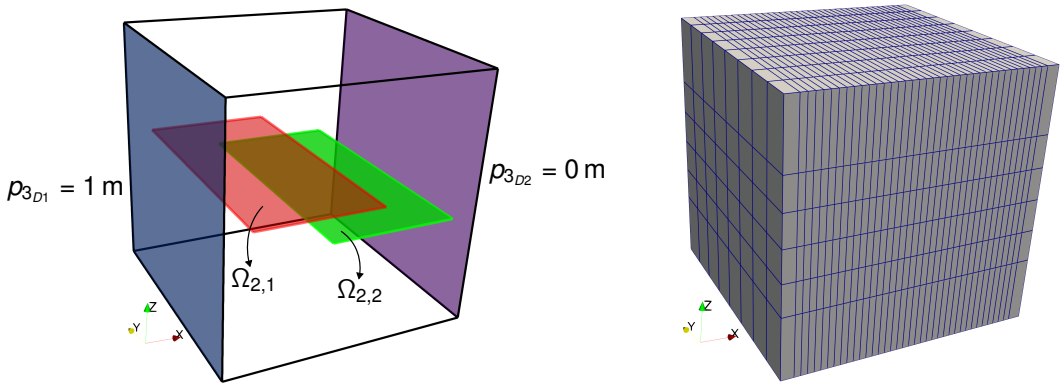

(a) Problem domain and boundary conditions. (b) Initial coarse mesh for the DFNMesh algorithm.

Figure 3. Problem with two fractures – domain and initial coarse mesh.

Figure 5 presents the flow results in the x-direction for each fracture and case along a line passing through the length of the fractures. It is observed that treating overlapping fractures with the actual permeability of the porous media aligns closely with the non-overlapping scenario. Conversely, when fractures in the overlapping region are assumed to have the same pressure (high $K_{(ij)}$), the flow in the x-direction in each fracture is overestimated. On the other hand, assuming that the fractures do not exchange flow with each other (low $K_{(ij)}$) results in an underestimation of the flow in the x-direction in each fracture.

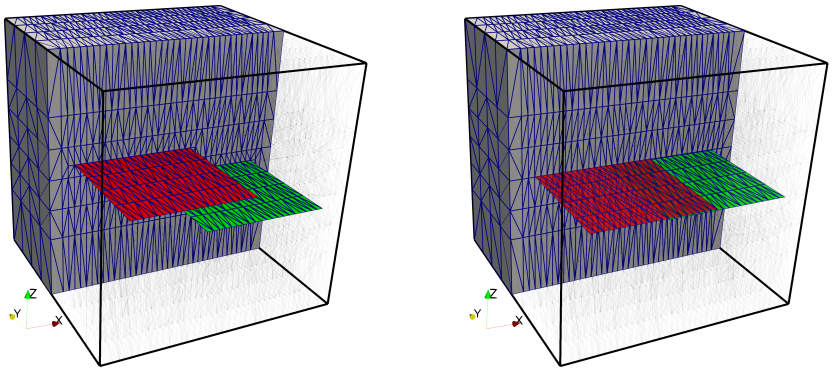

(a) Without snapping ($\epsilon_d < 0.1$ m). (b) With snapping ($\epsilon_d > 0.1$ m).

Figure 4. Problem with two fractures – meshes generated by the DFNMesh algorithm using different tolerances for snapping.

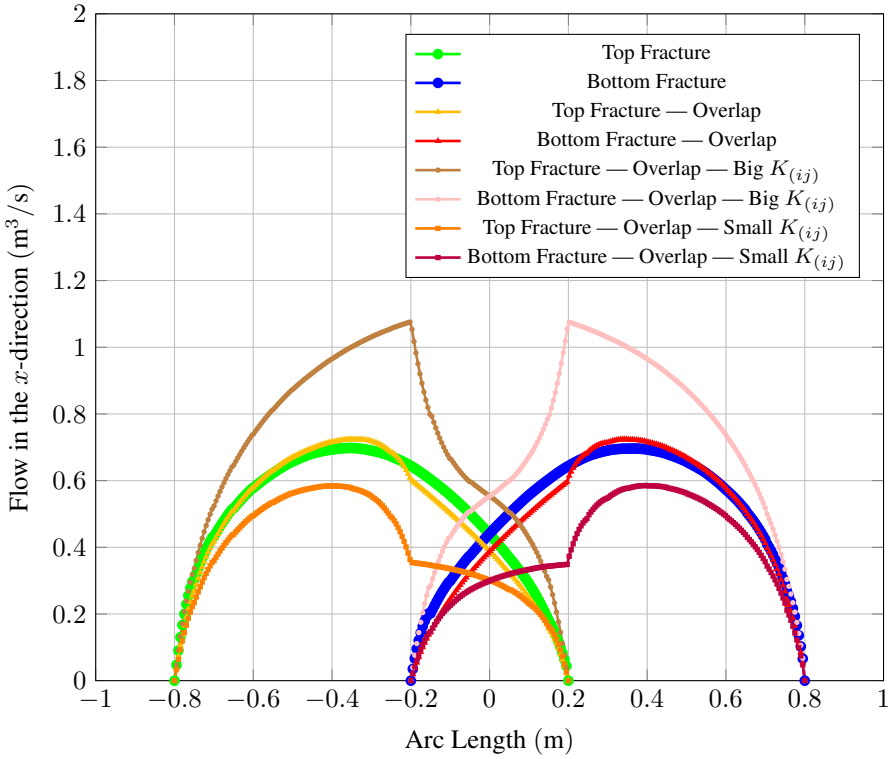

Figure 5. Flow in the x–direction along lines defined from $(-0.8\,\text{m}, 0\,\text{m})$ to $(0.2\,\text{m}, 0\,\text{m})$ for the top fracture and $(-0.2\,\text{m}, 0\,\text{m})$ to $(0.8\,\text{m}, 0\,\text{m})$ for the bottom fracture. Comparing cases without fracture overlap and with fractures overlap with different normal porous media permeabilities between the fractures.

3.2 Benchmark problem

As detailed in [16], this problem involves a network of 8 fractures within a cubic 3D domain, illustrated in Figure 6a. Building on the analysis conducted by [18], four different cases are examined, each varying in snapping tolerances. Case A provides the most precise description of the fractures, while Case D exhibits significant overlaps between fractures. Each fracture in the domain is labeled from f_1 to f_8, as depicted in Figure 6b.

Results of fluid entering and leaving fracture f_8 are shown in Figure 7, where it is observed that the treatment for overlapping fractures proposed here leads to a good representation of the fluid exchange between fractures even when the geometric fidelity is not very accurate (case D).

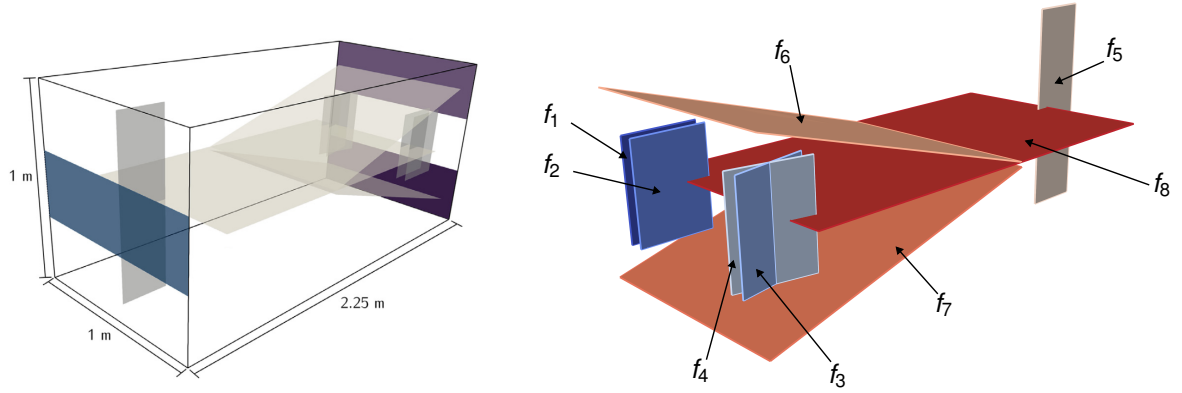

(a) Problem domain, network of 8 fractures, and boundary conditions of inflow (blue) and outflow (purple) of the benchmark problem [16].

(b) Labels adopted for each fracture in the domain.

Figure 6. Problem domain and fracture labels.

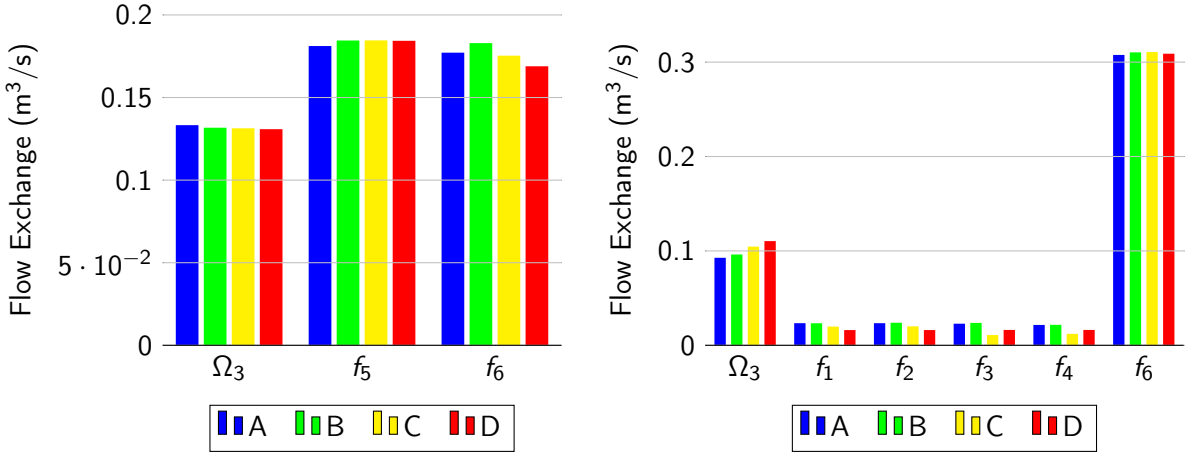

(a) Incoming flow

(b) Outgoing flow

Figure 7. Fluid flow exchange between fracture 8 (f_8), connecting fractures and volume (Ω_3) for mesh cases A, B, C and D.

4 Conclusions

This work analyzes a method for simulating flow in fractured porous media, emphasizing local conservation, which is crucial for this type of simulation [5]. The methodology presented addresses overlapping fractures by modeling only the transverse flow between them, adding minimal degrees of freedom to the global system of equations. The method's effectiveness is demonstrated through a simple example and a benchmark problem revealing that the proposed treatment for overlapping fractures in Section 2.1 accurately represents fluid exchange between fractures, even when geometric fidelity is less precise.

Acknowledgements. The authors gratefully acknowledge the support of EPIC – *Energy Production Innovation Center*, hosted by the University of Campinas (UNICAMP) and sponsored by Equinor Brazil and FAPESP – *São Paulo Research Foundation* (2017/15736-3). The authors also acknowledge the support of ANP - *Brazil's National Oil, Natural Gas and Biofuels Agency* through the R&D levy regulation. Acknowledgments are extended to the Center for Petroleum Studies (CEPETRO), School of Mechanical Engineering (FEM), and the School of Civil Engineering, Architecture and Urban Planning (FECFAU). Author P. R. B. Devloo (grants 305823/2017-5 and 309597/2021-8) thankfully acknowledges financial support from the CNPq - *Conselho Nacional de Desenvolvimento Científico e Tecnológico*. N. Shauer (scholarship 2021/03791-5) is grateful to FAPESP - *São Paulo Research Foundation*. J. B. Villegas acknowledges the financial support of the *Universidad Estatal Peninsula de Santa Elena*.

Authorship statement. The authors hereby confirm that they are the sole liable persons responsible for the authorship of this work, and that all material that has been herein included as part of the present paper is either the property (and authorship) of the authors, or has the permission of the owners to be included here.

References

[1] B. Singhal and R. Gupta. *Applied Hydrogeology of Fractured Rocks*, volume 2. Springer, 2010.
[2] B. Shah, D. Rajvanshi, and P. Sivasankar. A review of thermal enhanced oil recovery in naturally fractured reservoir. In *SPE International Conference on Unconventional Hydrocarbon Resources*, 2019.
[3] P. Angot, F. Boyer, and F. Hubert. Asymptotic and numerical modelling of flows in fractured porous media. *ESAIM: M2AN*, vol. 43, n. 2, pp. 239–275, 2009.
[4] V. Martin, J. Jaffré, and J. E. Roberts. Modeling fractures and barriers as interfaces for flow in porous media. *SIAM Journal on Scientific Computing*, vol. 26, n. 5, pp. 1667–1691, 2005.
[5] W. M. Boon, J. M. Nordbotten, and I. Yotov. Robust discretization of flow in fractured porous media. *SIAM Journal on Numerical Analysis*, vol. 56, n. 4, pp. 2203–2233, 2018.
[6] P. Angot. A model of fracture for elliptic problems with flux and solution jumps. *Comptes Rendus Mathematique*, vol. 337, n. 6, pp. 425–430, 2003.
[7] P. F. Antonietti, C. Facciolà, A. Russo, and M. Verani. Discontinuous galerkin approximation of flows in fractured porous media on polytopic grids. *SIAM Journal on Scientific Computing*, vol. 41, n. 1, pp. A109–A138, 2019.
[8] P. F. Antonietti, L. Formaggia, A. Scotti, M. Verani, and N. Verzott. Mimetic finite difference approximation of flows in fractured porous media. *ESAIM: M2AN*, vol. 50, n. 3, pp. 809–832, 2016.
[9] K. Brenner, J. Hennicker, R. Masson, and P. Samier. Gradient discretization of hybrid-dimensional Darcy flow in fractured porous media with discontinuous pressures at matrixfracture interfaces. *IMA Journal of Numerical Analysis*, vol. 37, n. 3, pp. 1551–1585, 2016.
[10] A. Fumagalli and E. Keilegavlen. Dual virtual element method for discrete fractures networks. *SIAM Journal on Scientific Computing*, vol. 40, n. 1, pp. B228–B258, 2018.
[11] E. Rivas, M. Parchei-Esfahani, and R. Gracie. A two-dimensional extended finite element method model of discrete fracture networks. *International Journal for Numerical Methods in Engineering*, vol. 117, n. 13, pp. 1263–1282, 2019.
[12] P. R. B. Devloo, W. Teng, and C. S. Zhang. Multiscale hybrid-mixed finite element method for flow simulation in fractured porous media. *CMES - Computer Modeling in Engineering and Sciences*, vol. 119, n. 1, pp. 145–163, 2019.
[13] E. Burman, P. Hansbo, and M. G. Larson. A cut finite element method for a model of pressure in fractured media. *Numerische Mathematik*, vol. 146, n. 4, pp. 783–818, 2020.
[14] L. H. Odsæter, T. Kvamsdal, and M. G. Larson. A simple embedded discrete fracture-matrix model for a coupled flow and transport problem in porous media. *Computer Methods in Applied Mechanics and Engineering*, vol. 343, pp. 572–601, 2019.
[15] B. Flemisch, I. Berre, W. Boon, A. Fumagalli, N. Schwenck, A. Scotti, I. Stefansson, and A. Tatomir. Benchmarks for single-phase flow in fractured porous media. *Advances in Water Resources*, vol. 111, pp. 239–258, 2018.
[16] I. Berre, W. M. Boon, B. Flemisch, A. Fumagalli, D. Gläser, E. Keilegavlen, A. Scotti, I. Stefansson, A. Tatomir, K. Brenner, S. Burbulla, P. Devloo, O. Duran, M. Favino, J. Hennicker, I.-H. Lee, K. Lipnikov, R. Masson, K. Mosthaf, M. G. C. Nestola, C.-F. Ni, K. Nikitin, P. Schädle, D. Svyatskiy, R. Yanbarisov, and P. Zulian. Verification benchmarks for single-phase flow in three-dimensional fractured porous media. *Advances in Water Resources*, vol. 147, pp. 103759, 2021.
[17] O. Durán, P. R. Devloo, S. M. Gomes, and F. Valentin. A multiscale hybrid method for darcy's problems using mixed finite element local solvers. *Computer Methods in Applied Mechanics and Engineering*, vol. 354, pp. 213–244, 2019.
[18] P. Lima, N. Shauer, J. B. Villegas, and P. R. Devloo. Dfnmesh: Finite element meshing for discrete fracture matrix models. *Advances in Engineering Software*, vol. 186, pp. 103545, 2023.